# Porous Spinel $Zn_xCo_{3-x}O_4$ Hollow Polyhedra Templated for High-Rate Lithium-Ion Batteries

**Renbing Wu,[†] Xukun Qian,[‡] Kun Zhou,[†,*] Jun Wei,[§] Jun Lou,[⊥] and Pulickel M. Ajayan[⊥]**

[†]School of Mechanical and Aerospace Engineering and [‡]School of Materials Science and Engineering, Nanyang Technological University, Singapore 639798, [§]Singapore Institute of Manufacturing Technology, Singapore 638075, and [⊥]Department of Mechanical Engineering and Materials Science, Rice University, Houston, Texas 77005, United States

**ABSTRACT** Nanostructured metal oxides with both anisotropic texture and hollow structures have attracted considerable attention with respect to improved electrochemical energy storage and enhanced catalytic activity. While synthetic strategies for the preparation of binary metal oxide hollow structures are well-established, the rational design and fabrication of complex ternary metal oxide with nonspherical hollow features is still a challenge. Herein, we report a simple and scalable strategy to fabricate highly symmetric porous ternary $Zn_xCo_{3-x}O_4$ hollow polyhedra composed of nanosized building blocks, which involves a morphology-inherited and thermolysis-induced transformation of heterobimetallic zeolitic imidazolate frameworks. When tested as anode materials for lithium-ion batteries, these hollow polyhedra have exhibited excellent electrochemical performance with high reversible capacity, excellent cycling stability, and good rate capability.

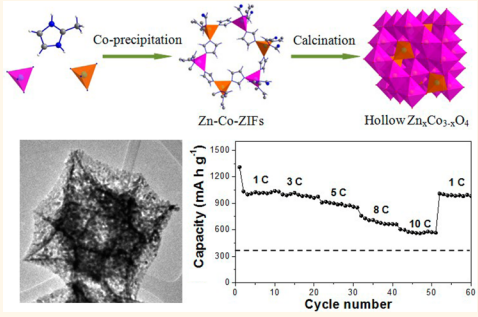


**KEYWORDS:** electrochemistry · hollow polyhedra · ternary oxides · metal−organic frameworks

Metal oxides with hollow and porous features have received increasing attention because of their unique structure-dependent properties that render them promising candidates in a wide range of applications, such as energy storage and conversion, catalysis, and biomedicine.[1−6] The most popular strategy to achieve hollow structures involves the coating of a shell on removable or sacrificial templates based on different principles including Kirkendall effect, galvanic replacement, and chemical etching.[7−12] This template-engaged approach has demonstrated effectiveness in forming hollow metal oxide particles with various shapes. Nevertheless, the general routes reported so far require tedious synthetic procedures, and the resulting hollow structures are limited to binary metal oxides. The design of a facile and reliable method for the rational synthesis of well-defined and high-symmetry ternary metal oxide hollow structures still remains a big challenge and may have great interest in the field of materials science.

Metal−organic frameworks are a novel class of porous materials consisting of metal ions coordinated to rigid organic molecules to form diverse architectures and have been proven to be a promising precursor or sacrificial template to construct the corresponding morphology-inherited hollow metal oxides.[13−23] For example, Prussian blue analogues have been utilized for selective synthesis of $Fe_2O_3$ microboxes and $Co_3O_4$ nanocages.[14−16] By using Cu-based MOFs as the sacrificial template, CuO and $CuO/Cu_2O$ hollow polyhedra have been prepared for lithium-ion batteries (LiBs).[19,20] The composition-tunable multiple ball-in-ball hybrid metal oxides have also been fabricated by taking advantage of the unique reactivity and thermal behavior of spherical MOFs.[22] Despite the great progress that has been made, there has rarely been success in generating high-symmetry complex ternary metal oxide hollow structures derived from MOFs, possibly due to additional difficulties ranging from the paucity of a well-defined MOF template containing homogeneity of different metal ions to the preservation of the shape with high residual stresses.

* Address correspondence to kzhou@ntu.edu.sg.

Received for review April 1, 2014 and accepted May 15, 2014.

**Published online May 15, 2014**
**10.1021/nn501783n**

In this work, we report a bottom-up procedure based on the coprecipitation of Zn and Co ions in the presence of 2-methylimidazolate to produce heterobimetallic zeolitic imidazolate frameworks (ZIFs), followed by a thermal decomposition process to form ternary spinel $Zn_xCo_{3-x}O_4$ ($0 < x \leq 1$) hollow polyhedra. ZIFs are considered as a new subclass of MOFs consisting of tetrahedral metal ions bridged by imidazolate linkers, which are structurally analogous to porous zeolites.[24] When evaluated as anode materials, the as-synthesized anisotropic $Zn_xCo_{3-x}O_4$ hollow polyhedra exhibit high lithium storage capacity and excellent rate capability in LiBs.

## RESULTS AND DISCUSSION

The overall synthetic process for the ternary $Zn_xCo_{3-x}O_4$ hollow polyhedra is schematized in Figure 1. The formation of bimetallic ZIFs with a unique polyhedral morphology was first achieved by the reaction of 2-methylimidazole with divalent Zn ions and Co ions in methanol solution at room temperature. The precipitated sample was designated as "Zn-Co-ZIF-*n*", where the "*n*" indicates the Zn/Co molar ratio in the reactants. After postannealing treatment, porous $Zn_xCo_{3-x}O_4$ hollow polyhedra with anisotropic texture could be readily obtained by a thermally induced oxidative decomposition process.

Zn-Co-ZIFs-*n* were examined by powder X-ray diffraction (XRD), as shown in Figure 2a. All Zn-Co-ZIFs-*n* exhibit strong diffraction peaks at similar positions, and all peaks match well with the simulated ZIF-8,[25] indicating that they have high crystallinity and pure-phase ZIF-8 structure. The morphologies of the Zn-Co-ZIFs-*n* were characterized by field-emission scanning electron microscopy (FESEM), and the representative FESEM images of Zn-Co-ZIFs-0.33 are shown in Figure 2b. It can be clearly observed that the formation of Zn-Co-ZIFs-0.33 particles has good uniformity with a size of ~1 $\mu$m. The magnified SEM image shown in Figure 2c reveals that these particles have high-symmetry geometry, and each of them is a regular rhombic dodecahedral crystal with 12 exposed {110} facets. When the Zn/Co molar ratio was changed to 0.25 and 0.5, the resulting products (Zn-Co-ZIFs-0.25 and Zn-Co-ZIFs-0.5) comprising evenly polyhedral crystals could still be obtained (Supporting Information Figure S1), respectively. The chemical compositions of Zn-Co-ZIFs-0.33 were analyzed by energy-dispersive X-ray spectroscopy (EDS), where both Zn and Co elements were found to be incorporated within the polyhedron. It should be mentioned that all the Zn:Co molar ratios within the bimetallic ZIFs were higher than those of corresponding reactants, which may be because $Zn^{2+}$ has a stronger coordination ability than $Co^{2+}$ (Figure S2). A combination of elemental analyses and the PXRD patterns of the as-synthesized samples indicated that the reaction of a 2-methylimidazole ligand with Zn and Co ions could result in bimetallic ZIFs as pure phase rather than a mixture of two homometallic ZIFs. To the best of our knowledge, the fabrication of well-defined heterobimetallic ZIFs with mixed Zn and Co ions has not been investigated previously.

The thermal behavior of bimetallic Zn-Co-ZIFs-0.33 was investigated by thermogravimetric analysis (TGA), as shown in Figure S3. It was found that the bimetallic ZIFs could be stable at ~400 °C. Above 400 °C, there was a significant weight loss of about 63.5%, which can be attributed to the escape of organic molecules by the thermal decomposition of Zn-Co-ZIFs. Based on the TGA results, the as-prepared bimetallic Zn-Co-ZIFs were first heated in nitrogen gas at 400 °C and then kept in air at the same temperature to obtain the final products. It was noticeable that the first thermal treatment in nitrogen gas was favorable for preserving the framework of ZIFs due to the fact that carbon generated during this process might act as a temporal buffer, preventing further contraction of ZIFs.[26] The crystallographic structure and phase of the annealed products were examined by XRD, and the results are

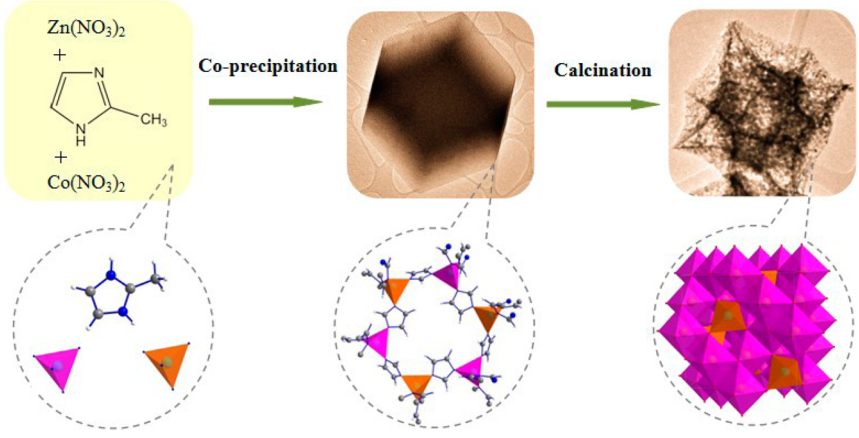


**Figure 1. Schematic illustration of the preparation of bimetallic ZIFs and their conversion to spinel $Zn_xCo_{3-x}O_4$ hollow polyhedra.**

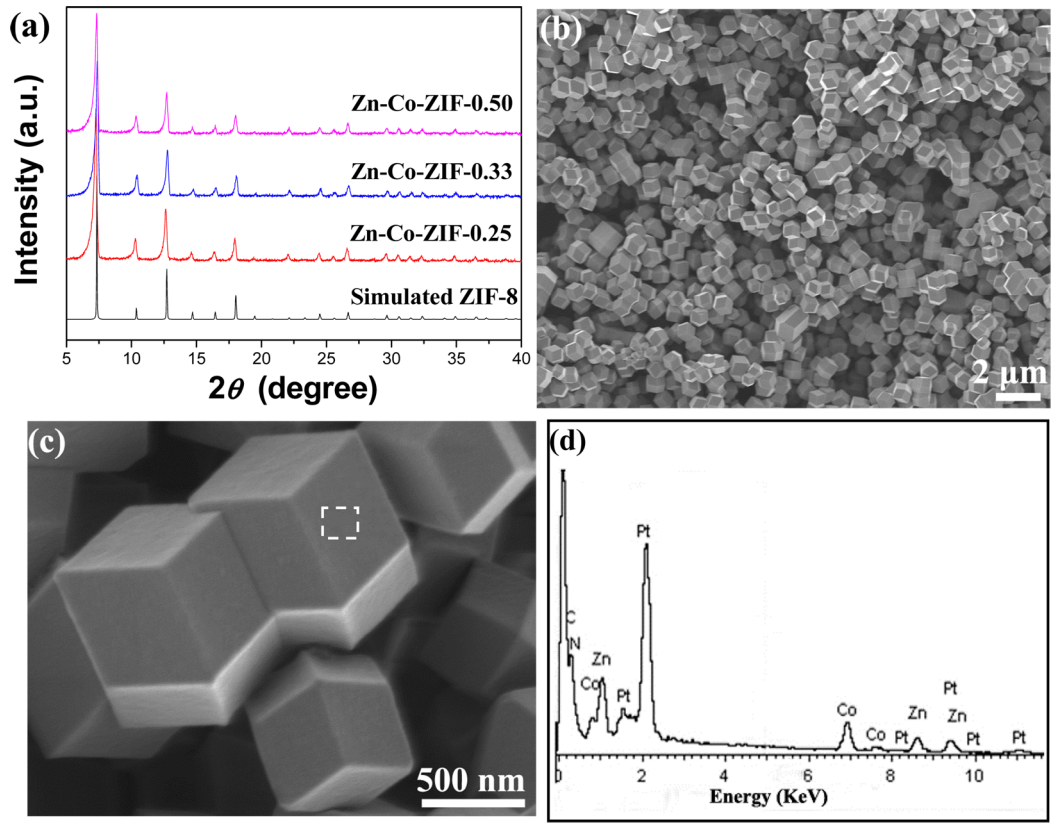


**Figure 2. (a) XRD patterns of Zn-Co-ZIFs; (b) low- and (c) high-magnification FESEM images of Zn-Co-ZIF-0.33; (d) EDS spectrum recorded from the area indicated by a white square in c.**

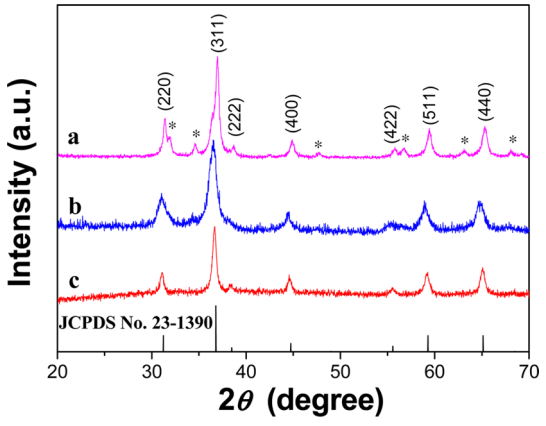


**Figure 3. XRD patterns of products prepared from (a) Zn-Co-ZIFs-0.50, (b) Zn-Co-ZIFs-0.33, and (c) Zn-Co-ZIFs-0.25, in which the signals of ZnO phase are marked with black asterisks. The vertical lines below the pattern correspond to the standard XRD pattern of $Zn_xCo_{3-x}O_4$ (JCPDS card no. 23-1390).**

shown in Figure 3. When Zn-Co-ZIFs-0.5 was used as precursor, the obtained product had the main phase of spinel $Zn_xCo_{3-x}O_4$ ($0 < x \leq 1$) (JCPDS card no. 23-1390) with a secondary phase ZnO. On the other hand, when Zn-Co-ZIFs-0.33 and Zn-Co-ZIFs-0.25 were used as precursor, respectively, both products were pure spinel $Zn_xCo_{3-x}O_4$ without the ZnO phase, indicating that all the zinc atoms were well incorporated into the $Co_3O_4$ lattice without phase separation. No other impurity peaks were observed in the XRD patterns, revealing a complete transformation of the precursor to metal oxides.

The detailed morphological and structural features of $Zn_xCo_{3-x}O_4$ were further characterized by FESEM and transmission electron microscopy (TEM). A typical FESEM image of the $Zn_xCo_{3-x}O_4$ products prepared from Zn-Co-ZIFs-0.33 is shown in Figure 4a, suggesting that they consist of uniform polyhedra without aggregation. A magnified FESEM image (Figure 4b) indicates that these polyhedra inherited well the size and rhombic dodecahedral shape of the Zn-Co-ZIFs precursor. The surface of polyhedra was very rough and composed of closely packed small nanoparticles with size of around 10 nm, as revealed by a high-resolution FESEM image (Figure 4c). Meanwhile, the EDS analysis of the polyhedral structure showed the Co/Zn atomic ratio of 2.16:1 (Figure S4). According to this ratio, $Zn_xCo_{3-x}O_4$ should have the form of $Zn_{0.95}Co_{2.05}O_4$. The hollow interior of these polyhedra was confirmed by TEM analysis. As shown in the TEM image (Figure 4d), there exists sharp contrast between the shells (dark) and interior cavities (light) of the polyhedra. The highly symmetric dodecahedral shell framework constructed by small subunits and the interparticle mesopores distributed throughout the shell could be observed more distinctly from the magnified TEM image (Figure 4e). It should be mentioned that the porous $Zn_xCo_{3-x}O_4$ hollow polyhedra could retain their

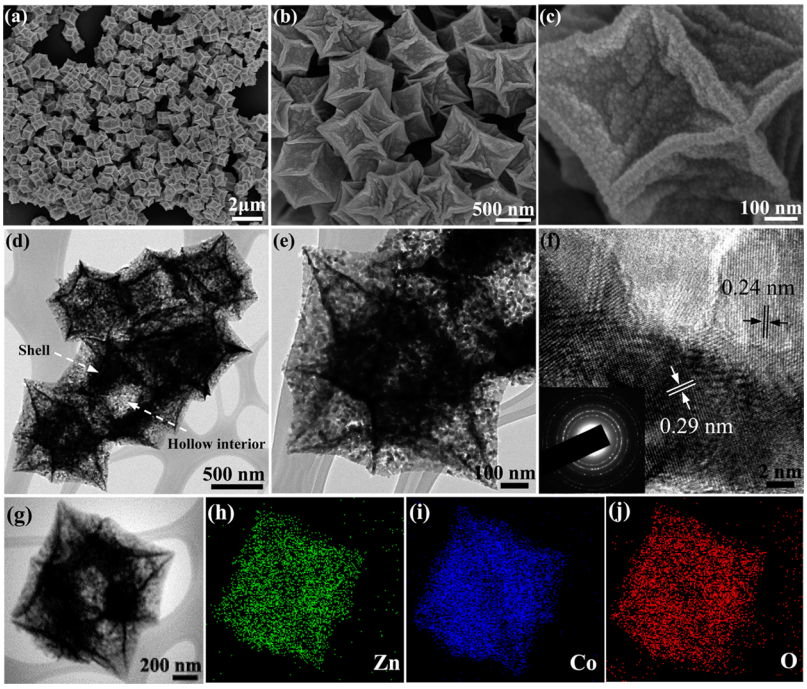


**Figure 4. $Zn_xCo_{3-x}O_4$ hollow polyhedra obtained by annealing Zn-Co-ZIFs-0.33: (a–c) FESEM images, (d,e) TEM images, (f) HRTEM image with inset showing the SAED pattern, (g) TEM image, and (h,i) EDX mapping images of a $Zn_xCo_{3-x}O_4$ hollow polyhedron.**

structural integrity even after ultrasonic dispersion. The selected area electron diffraction (SAED) and high-resolution TEM analyses further indicated the polycrystalline texture of $Zn_xCo_{3-x}O_4$ shells. The lattice fringes were visible, and the *d*-spacings of 0.29 and 0.24 nm were measured to correspond well to the (220) and (311) planes of cubic spinel $ZnCo_2O_4$. In addition, a large number of atomic steps or kinks could be found in the exterior surfaces of the small subunits that constructed the shells of the polyhedra. The elemental mapping analysis of a single hollow dodecahedron confirmed the coexistence and homogeneous dispersion of Zn, Co, and O elements within it (Figure 4g–j). The texture and porosity of the sample were also characterized by measuring nitrogen adsorption–desorption isotherms (Figure S5). The porous hollow structure gave rise to a high Brunauer–Emmett–Teller (BET) surface area of 65.58 $m^2\ g^{-1}$, which is much higher than that of the reported $ZnCo_2O_4$ nanostructures.[27−29] The pore-size distribution obtained using the Barrett–Joyner–Halenda (BJH) method revealed a bimodal distribution, with two narrow distributions centered at 4 and 9 nm. The release of generated gases due to the oxidation of carbon and nitrogen during thermal treatment resulted in small pores in dodecahedra, while the large pores could be attributed to the connection between some of the small pores. Such a hollow structure constructed by ultrafine subunits with bimodal mesopores is beneficial to providing sufficient surface area to facilitate electrochemical reactions and efficient penetration of the electrolyte into the active materials. Furthermore, even after ZIFs were annealed at an elevated temperature of 500 °C, the hollow dodecahedra morphology could still be well-preserved, suggesting good structural stability, whereas the surface became rougher due to the growth of the composed subunits (Figure S6).

As a ternary cobalt-based metal oxide, spinel $ZnCo_2O_4$ has been intensively investigated as a promising electrode material for LiBs because of its low cost, good environmental benignity, and high theoretical capacity.[27−32] Motivated by the advantage of porous hollow structures in LiBs, electrochemical measurements were carried out to evaluate the performance of the as-prepared porous $Zn_xCo_{3-x}O_4$ hollow dodecahedra. Figure 5a depicts the first, second, and tenth cycle discharge–charge voltage profiles of the $Zn_xCo_{3-x}O_4$ hollow dodecahedra at a current density of 100 mA $g^{-1}$ in the potential range from 0.01 to 3 V. It can be seen that the first discharge curve exhibits a clear potential plateau at about 1 V, and this potential plateau shifts upward close to 1.3 V and becomes steeper in the subsequent discharge curves. This observation is similar to those previously reported.[27,28] The initial discharge and charge capacities are 1272 and 969 mA h $g^{-1}$, respectively, corresponding to a Coulombic efficiency of 76.2%. The first cycle irreversible capacity loss of 23.8% could be attributed to the formation of solid electrolyte interphase and the reduction of metal oxide to metal with $Li_2O$ formation. The curve of capacity *versus* cycle number at a current density of 100 mA h $g^{-1}$ is shown in Figure 5b. From the second cycle onward, the as-prepared $Zn_xCo_{3-x}O_4$ hollow dodecahedra exhibit excellent cyclic capacity retention upon prolonged cycling and a reversible capacity as high as 990 mA h $g^{-1}$

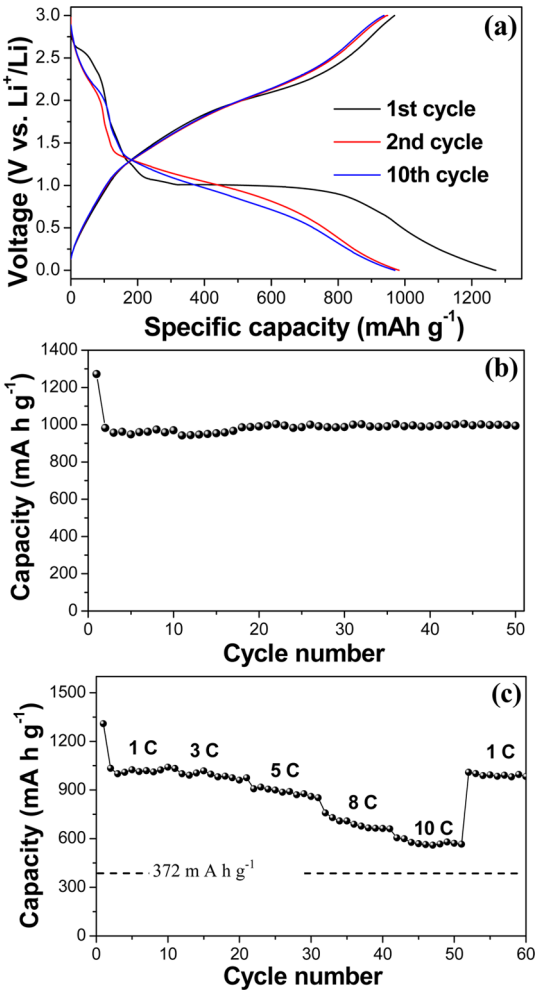


**Figure 5. Electrochemical properties of the porous $Zn_xCo_{3-x}O_4$ hollow polyhedra as electrodes in LiBs: (a) charge–discharge voltage profiles at a current density of 100 mA $g^{-1}$, (b) discharge capacities *versus* cycle number at a current density of 100 mA $g^{-1}$, and (c) rate capability at various current rates between 1 and 10 C.**

can still be retained at the end of 50 charge–discharge cycles. Besides the good specific capacity and excellent cyclability, the rate capability is also crucial for many practical applications of LiBs such as electrical vehicles and power tools. The rate capability of the $Zn_xCo_{3-x}O_4$ hollow polyhedra was evaluated at various current densities from 1 to 10 C (1 C = 900 mA h $g^{-1}$), as presented in Figure 5c. As can be seen, it shows good rate capability with the average discharge capacities of 1020, 988, 886, and 692 mA h $g^{-1}$ at 1, 3, 5, and 8 C, respectively. Even at the high rate of 10 C, the $Zn_xCo_{3-x}O_4$ hollow polyhedra electrode could still deliver a specific capacity of 575 mA h $g^{-1}$, which is much higher than the theoretical capacity of graphite electrodes (372 mA h $g^{-1}$). More importantly, after the high-rate charge–discharge cycling, a capacity of 991 mA h $g^{-1}$ could be resumed upon the reduction of the rate to 1 C, indicating the good reversibility of the electrode materials. Such a remarkable high-rate performance is significantly superior to that of most $ZnCo_2O_4$ nanostructures reported previously.[27–30]

The excellent electrochemical performance of $Zn_xCo_{3-x}O_4$ hollow polyhedra might be related to their unique structural features in several aspects. First, the building subunits with sizes of only a few nanometers in polyhedra not only facilitate the transport of Li ions and electrons but also render a high surface area, which is critical to the rate capability. Second, the porous shells and the void space within the hollow polyhedra can endure the volume expansion/contraction during the $Li^+$-ion insertion/extraction processes, hence partly alleviating the pulverization problem and improving the cycling stability. As shown in Figures S7, $Zn_xCo_{3-x}O_4$ polyhedra still could preserve the shape integrity and hollow feature after 50 cycles. Third, the high-symmetry hollow structures assembled by nanosized subunits in the shell may provide more freedom to produce atomic steps than asymmetrical structures. The presence of a high density of atomic steps in the facets may catalytically facilitate the reaction of Li with $Zn_xCo_{3-x}O_4$ and thus improve the electrochemical performance of the product.[33] Finally, the hollow architecture would effectively suppress the aggregation of the primary nanoparticles and their dissolution into electrolytes.

## CONCLUSION

In summary, we have developed an efficient ZIFs templating approach for the preparation of ternary porous $Zn_xCo_{3-x}O_4$ hollow polyhedra. This approach involves the bottom-up formation of heterobimetallic ZIFs template by the coprecipitation of Zn and Co ions in the presence of 2-methylimidazolate and the subsequent thermal decomposition of the template at appropriate temperature. The as-synthesized $Zn_xCo_{3-x}O_4$ hollow polyhedra inherited well the morphology of ZIFs and were composed of nanosized subunits in the shell. When evaluated as electrode material for LiBs, the high-symmetry porous $Zn_xCo_{3-x}O_4$ hollow polyhedra exhibited excellent cycling stability and rate capability. We anticipate that the low cost and convenient method demonstrated in this work could be extended to the fabrication of other ternary metal oxide hollow structures with anisotropic texture that may hold great promise for the construction of advanced electrodes in energy storage and conversion.

## EXPERIMENTAL METHODS

**Preparation of Bimetallic ZIFs.** All chemicals and solvents were purchased from commercial sources and used without purification. In a typical synthesis process, $Co(NO_3)_2 \cdot 6H_2O$ (582 mg, 2 mmol) and $Zn(NO_3)_2 \cdot 6H_2O$ (297 mg, 1 mmol) were dissolved in 30 mL of methanol (MeOH) to form a clear solution,

which was subsequently poured into 10 mL of MeOH containing 2-methylimidazole (984 mg, 12 mmol). After thorough mixing, the resulting solution was incubated at room temperature for 24 h. The as-obtained precipitates were centrifuged and washed with ethanol several times, resulting in so-called Zn-Co-ZIF-0.50. Similarly, for the synthesis of Zn-Co-ZIF-0.25 and Zn-Co-ZIF-0.33, the procedures were carried out except that the Zn/Co molar ratios were 0.25 and 0.33, respectively.

**Synthesis of $Zn_xCo_{3-x}O_4$ Hollow Polyhedra.** The powder of Zn-Co-ZIFs-*n* was placed in a tube furnace and then heated to 400 °C for 30 min with a ramp of 5 °C $min^{-1}$ under nitrogen gas flow. After that, the nitrogen gas was switched off, and the furnace was still kept in air at this temperature for another 30 min. Finally, the product was taken out and showed its color changed from pink to black.

**Characterization.** The phase purity of all the products was characterized by X-ray powder diffractometer (Bruker D8 Advance) with Cu Kα radiation ($\lambda$ = 1.5406 Å). The morphology and structure of the products were examined by field-emission scanning electron microscopy (FESEM, JEOL JSM-7600F) and transmission electron microscopy (TEM, JEOL JSM-2100F), respectively. Energy-dispersive X-ray (EDX) analysis and elemental mapping were taken with the X-ray spectroscopy attached to the JSM-7600F and JEM-2100F, respectively. The thermogravimetric analysis measurement was carried out on a Shimadzu-60 thermoanalyzer with a heating rate of 10 °C $min^{-1}$ under a nitrogen atmosphere. The BET specific surface areas of products were calculated from the results of nitrogen physisorption at 77 K using a Quantachrome Instruments Autosorb AS-6B equipment.

**Electrochemical Measurements.** Electrochemical measurements were performed at room temperature based on a coin-type half-cell configuration. The working electrode was prepared by dispersing active materials, super-P carbon black, and polyvinylidene fluoride in *N*-methyl-2 pyrrolidinone solvent with a weight ratio of 80:10:10. The resulting slurry was spread on Cu foil and dried at 60 °C for 12 h. The coin cells were assembled in an argon-filled glovebox using lithium metal as counter electrode, Celgard2400 membrane as the separator, and 1 M $LiPF_6$ in a mixture of ethylene carbonate and dimethyl carbonate (1:1 in volume) as the electrolyte. The galvanostatic charge–discharge tests were performed on a NEWARE multichannel battery test system with a cutoff voltage window of 0.01–3.0 V *vs* $Li^+$/Li.

*Conflict of Interest:* The authors declare no competing financial interest.

*Acknowledgment.* This work was financially supported by the Start-up Grant of the Nanyang Technological University, Singapore (Grant No. SUG 10/10), and the Agency for Science, Technology and Research, Singapore (SERC Grant No. 112 290 4015).

*Supporting Information Available:* Additional FESEM images, TEM image, EDS spectra and element analysis, TGA curve, $N_2$ adsorption–desorption isotherms. This material is available free of charge via the Internet at http://pubs.acs.org.

## REFERENCES AND NOTES

1. Wang, Z. Y.; Zhou, L.; Low, X. W. Metal Oxide Hollow Nanostructures for Lithium-Ion Batteries. *Adv. Mater.* **2012**, *24*, 1903–1911.
2. An, K.; Hyeon, T. Synthesis and Biomedical Applications of Hollow Nanostructures. *Nano Today* **2009**, *4*, 359–373.
3. Gyger, F.; Hubner, M.; Feldmann, C.; Barsan, N.; Weimar, U. Nanoscale $SnO_2$ Hollow Spheres and Their Application as a Gas-Sensing Material. *Chem. Mater.* **2010**, *22*, 4821–4827.
4. Liu, S. W.; Yu, J. G.; Jaroniec, M. Tunable Photocatalytic Selectivity of Hollow $TiO_2$ Microspheres Composed of Anatase Polyhedra with Exposed {001} Facets. *J. Am. Chem. Soc.* **2010**, *132*, 11914–11916.
5. Shin, J. M.; Anisur, R. M.; Ko, M. K.; Im, G. H.; Lee, J. H.; Lee, I. S. Hollow Manganese Oxide Nanoparticles as Multifunctional Agents for Magnetic Resonance Imaging and Drug Delivery. *Angew. Chem., Int. Ed.* **2009**, *48*, 321–324.
6. Phan, V. N.; Lim, E.; Kim, T.; Kim, M.; Choi, Y.; Kim, B.; Lee, M.; Oh, A.; Jin, J.; Chae, Y.; *et al.* A Highly Crystalline Manganese-Doped Iron Oxide Nanocontainer with Predesigned Void Volume and Shape for Theranostic Applications. *Adv. Mater.* **2013**, *25*, 3202–3208.
7. Wang, W. S.; Dahl, M.; Yin, Y. D. Hollow Nanocrystals through the Nanoscale Kirkendall Effect. *Chem. Mater.* **2013**, *25*, 1179–1189.
8. Mel, A. E.; Buffiere, M.; Tessier, P. Y.; Konstantinidis, S.; Xu, W.; Du, K.; Wathuthanthri, I.; Choi, C. H.; Bittencourt, C.; Snyders, R. Highly Ordered Hollow Oxide Nanostructures: The Kirkendall Effect at the Nanoscale. *Small* **2013**, *9*, 2838–2843.
9. Wang, Z. Y.; Luan, D.; Li, C. M.; Su, F.; Madhavi, S.; Boey, F. Y. C.; Low, X. W. Engineering Nonspherical Hollow Structures with Complex Interiors By Template-Engaged Redox Etching. *J. Am. Chem. Soc.* **2010**, *132*, 16271–16277.
10. Nai, J. W.; Tian, Y.; Guan, X.; Guo, L. Pearson's Principle Inspired Generalized Strategy for the Fabrication of Metal Hydroxide and Oxide Nanocages. *J. Am. Chem. Soc.* **2013**, *135*, 16082–16091.
11. Oh, M. H.; Yu, T.; Yu, S. H.; Lim, B.; Ko, K. T.; Willinger, M. G.; Seo, D. H.; Kim, B. H.; Cho, M. G.; Park, J. H. Galvanic Replacement Reactions in Metal Oxide Nanocrystals. *Science* **2013**, *340*, 964–968.
12. Xia, X. H.; Wang, Y.; Ruditskiy, A.; Xia, Y. N. Galvanic Replacement: A Simple and Versatile Route to Hollow Nanostructures with Tunable and Well-Controlled Properties. *Adv. Mater.* **2013**, *25*, 6313–6333.
13. Jiang, H. L.; Xu, Q. Porous Metal–Organic Frameworks as Platforms for Functional Applications. *Chem. Commun.* **2011**, *47*, 3351–3370.
14. Zhang, L.; Wu, H. B.; Madhavi, S.; Hng, H. H.; Lou, X. W. Formation of $Fe_2O_3$ Microboxes with Hierarchical Shell Structures from Metal–Organic Frameworks and Their Lithium Storage Properties. *J. Am. Chem. Soc.* **2012**, *134*, 17388–17391.
15. Yan, N.; Hu, L.; Li, Y.; Wang, Y.; Zhang, H.; Hu, X. Y.; Kong, X. K.; Chen, Q. W. $Co_3O_4$ Nanocages for High-Performance Anode Material in Lithium-Ion Batteries. *J. Phys. Chem. C* **2012**, *116*, 7227–7235.
16. Hu, M.; Belik, A. A.; Imura, M.; Mibu, K.; Tsujimoto, Y.; Yamauchi, Y. Synthesis of Superparamagnetic Nanoporous Iron Oxide Particles with Hollow Interiors by Using Prussian Blue Coordination Polymers. *Chem. Mater.* **2012**, *24*, 2698–2707.
17. Risset, O. N.; Knowles, E. S.; Ma, S. Q.; Meisel, M. W.; Talham, D. R. RbjMk[Fe(CN)$_6$] (M=Co, Ni) Prussian Blue Analogue Hollow Nanocubes: A New Example of a Multilevel Pore System. *Chem. Mater.* **2013**, *25*, 42–47.
18. Zhang, L.; Wu, H. B.; Lou, X. W. MOFs-Derived General Formation of Hollow Structures with High Complexity. *J. Am. Chem. Soc.* **2013**, *135*, 10664–10672.
19. Wu, R. B.; Qian, X. K.; Yu, F.; Liu, H.; Zhou, K.; Huang, Y. Z. MOFs-Templated Formation of Porous CuO Hollow Octahedra for Lithium-Ion Battery Anode Materials. *J. Mater. Chem. A* **2013**, *1*, 11126–11129.
20. Hu, L.; Huang, Y. M.; Zhang, F. P.; Chen, Q. W. CuO/$Cu_2O$ Composite Hollow Polyhedrons Fabricated from Metal–Organic Framework Templates for Lithium-Ion Battery Anode with a Long Cycling Life. *Nanoscale* **2013**, *5*, 4186–4190.
21. Wu, R. B.; Qian, X. K.; Rui, X. H.; Liu, H.; Yadian, B.; Zhou, K.; Wei, J.; Yan, Q. Y.; Feng, X. Q.; Long, Y.; *et al.* Zeolitic Imidazolate Framework 67-Derived High Symmetric Porous $Co_3O_4$ Hollow Dodecahedra with Highly Enhanced Lithium Storage Capability. *Small* **2014**, *10*, 1932–1938.
22. Cho, W.; Lee, Y. H.; Lee, H. J.; Oh, M. Multi Ball-In-Ball Hybrid Metal Oxides. *Adv. Mater.* **2011**, *23*, 1720–1723.
23. Park, J. U.; Lee, H. J.; Cho, W.; Jo, C.; Oh, M. Facile Synthetic Route for Thickness and Composition Tunable Hollow Metal Oxide Spheres from Silica-Templated Coordination Polymers. *Adv. Mater.* **2011**, *23*, 3161–3163.
24. Phan, A.; Doonan, C. J.; Uribe-Romo, F. J.; Knobler, C. B.; O'Keeffe, M.; Yaghi, O. M. Synthesis, Structure, and Carbon Dioxide Capture Properties of Zeolitic Imidazolate Frameworks. *Acc. Chem. Res.* **2010**, *43*, 58–67.

25. Banerjee, R.; Phan, A.; Wang, B.; Knobler, C.; Furukawa, H.; O'Keeffe, M.; Yaghi, O. M. High-Throughput Synthesis of Zeolitic Imidazolate Frameworks and Application to $CO_2$ Capture. *Science* **2008**, *319*, 939–943.
26. Xu, X. D.; Cao, R. G.; Jeong, S.; Cho, J. Spindle-like Mesoporous α-$Fe_2O_3$ Anode Material Prepared from MOF Template for High-Rate Lithium Batteries. *Nano Lett.* **2012**, *12*, 4988–4991.
27. Li, J. F.; Wang, J. Z.; Wexler, D.; Shi, D. Q.; Liang, J. W.; Liu, H. K.; Xiong, S. L.; Qian, Y. T. Simple synthesis of Yolk-Shelled $ZnCo_2O_4$ Microspheres towards Enhancing The Electrochemical Performance of Lithium-Ion Batteries in Conjunction with a Sodium Carboxymethyl Cellulose Binder. *J. Mater. Chem. A* **2013**, *1*, 15292–15299.
28. Hu, L. L.; Qu, B. H.; Li, C. C.; Chen, Y. J.; Mei, L.; Lei, D. N.; Chen, L. B.; Li, Q. H.; Wang, T. H. Facile Synthesis of Uniform Mesoporous $ZnCo_2O_4$ Microspheres as a High-Performance Anode Material for Li-Ion Batteries. *J. Mater. Chem. A* **2013**, *1*, 5596–5602.
29. Qu, B. H.; Hu, L. L.; Li, Q. H.; Wang, Y. G.; Chen, L. B.; Wang, T. H. High-Performance Lithium-Ion Battery Anode by Direct Growth of Hierarchical $ZnCo_2O_4$ Nanostructures on Current Collectors. *ACS Appl. Mater. Interfaces* **2014**, *6*, 731–736.
30. Sharma, Y.; Sharma, N.; Rao, G. V. S.; Chowdari, B. V. R. Nanophase $ZnCo_2O_4$ as a High Performance Anode Material for Li-Ion Batteries. *Adv. Funct. Mater.* **2007**, *17*, 2855–2861.
31. Liu, B.; Zhang, J.; Wang, X. F.; Chen, G.; Chen, D.; Zhou, C. W.; Shen, G. Z. Hierarchical Three-Dimensional $ZnCo_2O_4$ Nanowire Arrays/Carbon Cloth Anodes for a Novel Class of High-Performance Flexible Lithium-Ion Batteries. *Nano Lett.* **2012**, *12*, 3005–3011.
32. Choi, S. H.; Kang, Y. C. Yolk-Shell, Hollow, and Single-Crystalline $ZnCo_2O_4$ Powders: Preparation Using a Simple One-Pot Process and Application in Lithium-Ion Batteries. *ChemSusChem* **2013**, *6*, 2111–2116.
33. Liu, D. Q.; Wang, X.; Wang, X. B.; Tian, W.; Bando, Y.; Golberg, D. $Co_3O_4$ Nanocages with Highly Exposed {110} Facets for High-Performance Lithium Storage. *Sci. Rep.* **2013**, *3*, 2543.